Journal of Science and Transport Technology
Journal homepage: https://jstt.vn/index.php/en

Free vibration and buckling analysis of bidirectional functionally graded plates with integrated piezoelectric layers

Huu-Quoc Tran, Van-Tham Vu*
Hanoi University of Civil Engineering, 55 Giai Phong Road, Bach Mai, Hanoi 100000, Vietnam

Article info
Type of article:
Original research paper

DOI:
https://doi.org/10.58845/jstt.utt.2026.en.6.1.48-66

***Corresponding author:**
Email address:
thamvv@huce.edu.vn

Received: 29/10/2025
Received in Revised Form: 21/11/2025
Accepted: 27/01/2026

Abstract: In this paper, the vibration and buckling of functionally graded material plates with integrated piezoelectric layers are investigated. The material properties of the plate are assumed to vary along both the length and thickness directions (2D-FGM) according to a power-law while the electric potential in each piezoelectric layer varies linearly along the thickness direction. To perform this analysis, a finite element model based on the higher-order shear deformation refined plate theory (HSDT-4) and four-node rectangular element is developed. The governing equations are obtained by applying Hamilton's principle. The numerical results have demonstrated the convergence, accuracy and reliability of the established model. In addition, the influence of material parameters, geometry and mechanical boundary conditions on the vibration frequency and critical force of the 2D-FGM/PIE plate under both closed-circuit (Clocc) and open-circuit (Opcc) conditions is investigated and evaluated in detail.

Keywords: 2D-FGM, Piezoelectric layers, Free vibration, Buckling behavior, High-order refined plate theory, FEM.

1. Introduction

With the rapid development of science and technology, in recent decades, many new materials have been invented and used to meet the increasingly stringent demands of practical applications. Among them, functionally graded material (FGM) is the most notable material. Thanks to its smooth and continuous transformation properties in one or more directions in the physical space and its high customizability, FGM is widely used in many fields such as aviation, aerospace, automobiles, mechanics and civil engineering. In addition, combining FGM with other materials to create a complex structure has also been a trend in recent years. For example, combining FGM with piezoelectric materials can create a smart and promising structure for many applications, and thus making the study of vibration and stability of FGM plates with piezoelectric layers necessary for safe designs.

Due to their promising applications, the synergistic combination of FGMs and piezoelectric materials in structural design has recently attracted considerable attention [1]. As a result, extensive research efforts have been reported on the modeling and analysis of such FGM-piezoelectric structures. The dynamics of piezoelectric FGM plates were explored by Rouzegar and Abad [2], who used the improved higher-order shear deformation theory (HSDT-4) and the Navier solution method to analyze free vibration. Meanwhile, a different approach was taken by

Askari Farsangi and Saidi [3], who utilized the Levy method to derive analytical solutions for similar plates with surface-bonded piezoelectric layers. Using an exact solution approach, Zhong and Yu [4] addressed the forced and free vibration of rectangular piezoelectric FGM plates with exponentially graded material properties. Using the spectral element method, Abad and Rouzegar [5] carried out further analysis of Levy-type FGM plates bonded with piezoelectric layers. The bending, free vibration, and dynamic responses of piezoelectric FGM plates under coupled mechanical, thermal, and electrical loading were analyzed by Behjat et al. [6] via FEM employing FSDT. Extending this line of research, Zhang et al. [7] investigated the static and dynamic responses of CNT-reinforced FGM plates with piezoelectric layers employing nonlinear FEM within the FSDT framework. Using a four-variable refined theory, Rouzegar and Davoudi [8] formulated a finite element method to analyze the forced vibration of viscoelastic composite laminates actuated by piezoelectric layers. More recently, electromechanical models were developed by Aghakhani et al. [9] and Motlagh et al. [10] to study the dynamic responses of FGM panels and plates with multiple piezoelectric patches on their surfaces. These studies, however, primarily focused on unidirectional FGMs, where material properties vary only in the thickness direction.

Recent studies have increasingly focused on bidirectional functionally graded material (2D-FGM), in which material properties vary simultaneously along both the length and thickness directions, offering enhanced flexibility in structural design. In particular, the mechanical behavior of 2D-FGM plates has been widely investigated. Van Do et al. [11] used the FEM with a newly developed third-order shear deformation theory to predict the static deflection and buckling loads of variable-thickness plates. A bending and deflection study of three-layered porous FGM piezoelectric plates resting on an elastic foundation and exposed to thermal and electrical loading under various boundary conditions was conducted by Harsha and Kumar [12]. Using the modified first-order shear deformation theory, the study employed a finite element method with nine-node higher-order elements and solved it via an improved iterative technique. Hashemi and Jafari [13] conducted an analysis of the nonlinear vibration of rectangular plates based on the first-order shear deformation theory and an analytical technique. Lieu et al. [14, 15] employed isogeometric analysis (IGA) based on NURBS and higher-order shear deformation theories to investigate their static response, in-plane vibration, and buckling characteristics. More recently, Li et al. [16] proposed an IGA model based on the first-order shear deformation theory to study the flexural, vibration, and buckling behavior of porous 2D-FGM plates.

Based on the preceding literature review, the research concerning the vibration and stability analysis of 2D-FGM plates incorporating piezoelectric layers is still insufficient. To bridge this knowledge gap, this study introduces a finite element model utilizing the improved high-order plate theory for the analysis of free vibration and buckling in 2D-FGM/PIE plates. The accuracy of the model is verified through numerical examples comparing the calculated results with the published results of other authors. Some new results are also performed to evaluate the influence of material parameters, geometry and electrical boundary conditions as well as mechanical boundary conditions on the vibration response and stability of the 2D-FGM/Pie plate.

2. Problem description

2.1. Model of 2D-FGM plates with integrated piezoelectric layers

A 2D-FGM plate with length a, width b, and core thickness h_c is considered. Two piezoelectric layers, each of thickness h_p, are perfectly bonded to the top and bottom surfaces of the plate. The Cartesian coordinate system is adopted for the model, as depicted in Fig. 1.

2.2. Effective material properties of the 2D-FGM

plate

In this study, the plate consists of two constituent materials: a ceramic phase (c) and a metallic phase (m). The effective properties of the plate are calculated using the following expression:

$$P(x,z) = P_c V_c(x,z) + P_m V_m(x,z) \quad (1)$$

where $P(x,z)$ is the material property (including Young's modulus, Poisson's ratio, and density) that varies in two directions, and $V_c(x,z)$ and $V_m(x,z)$, respectively, are the volume fractions of the ceramic and metal and they are determined as follows:

$$V_c(x,z) = \left(\frac{1}{2} + \frac{z}{h_c}\right)^{p_z} \left(1 - \frac{x}{2a}\right)^{p_x}; \quad V_m(x,z) = 1 - V_c(x,z). \quad (2)$$

in which, p_x and p_z being the volume fraction exponents corresponding to the longitudinal and thickness directions.

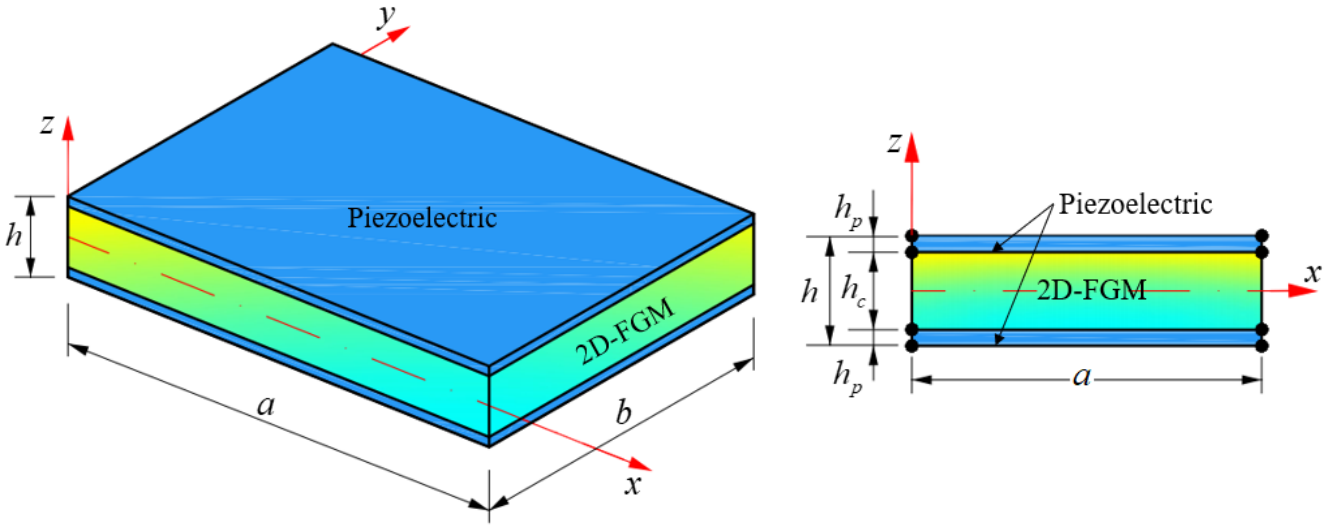

(a) Geometry and coordinate (b) Layer configuration

Fig. 1. Model of a 2D-FGM/Pie plate integrated with piezoelectric layers

3. Finite element formulation

In this study, the Higher-order Shear Deformation Refined Plate Theory with 4 displacement variables (HSDT-4) is adopted to approximate the displacement components. The selection of HSDT-4 is strategic because this theory naturally satisfies the zero transverse shear stress condition at the top and bottom free surfaces of the plate, thereby eliminating the need for a shear correction factor. Furthermore, the electric potential is assumed to be linearly distributed along the thickness of each piezoelectric layer [17]:

$$u = u_0 - z w_{b,x} - \Re w_{s,x}$$
$$v = v_0 - z w_{b,y} - \Re w_{s,y}$$
$$w = w_b + w_s \quad (3)$$
$$\Phi^t = \frac{2z - h_c}{2h_p}\phi^t = Z^t\phi^t$$
$$\Phi^b = -\frac{2z + h_c}{2h_p}\phi^b = Z^b\phi^b$$

here, u_0 and v_0 represent the horizontal displacements of a point on the mid-plane, while w_b and w_s denote the deflection components due to bending moments and shear forces, respectively. The function $\Re$ is the shape function governing the distribution of transverse shear stress through the plate's thickness, with a specific value of $\Re = z\left[-\frac{1}{8} + \frac{2}{3}\left(\frac{z}{h}\right)^2\right]$ selected for the present study.

The stress-strain relationship in a 2D-FGM/Pie plate is determined as follows:

$$\begin{Bmatrix} \sigma \\ D_e \end{Bmatrix} = \begin{bmatrix} C_e & -e^T \\ e & p \end{bmatrix} \begin{Bmatrix} \varepsilon \\ E \end{Bmatrix} \quad (4)$$

in the formulation, the stress vector $\{\sigma\}$ and dielectric displacement vector $\{D_e\}$ are related to the strain $\{\varepsilon\}$ and electric field $\{E\}$, with $[C_e]$, $[p]$, and $[e]$ representing the elastic, dielectric, and piezoelectric matrices, respectively.

Using four-node rectangular elements, the displacements u_0, v_0 are approximated with Lagrange functions (N) and the deflections w_b, w_s with Hermit functions (H). Subsequently, the displacement field can be expressed as follows:

$$\bar{u} = N_u d \tag{5}$$

$$\bar{\Phi} = N_\phi \Phi \tag{6}$$

where: $\bar{u} = \{u \quad v \quad w\}^T$ is the displacement of any point in the plate. $d = \{d_1 \quad d_2 \quad d_3 \quad d_4\}^T$ is element nodal displacement vector, with its components as shown below:

$$\{d_i\} = \{u_0 \; v_0 \; w_b \; w_{b,x} \; w_{b,y} \; w_s \; w_{s,x} \; w_{s,y}\}^T \tag{7}$$

$\bar{\Phi} = \{\Phi^t \quad \Phi^b\}^T$ is the electric potential of any point in the plate.

$\Phi = \{\Phi_1 \quad \Phi_2 \quad \Phi_3 \quad \Phi_4\}^T$ is the element nodal electric potential whose components are $\Phi_i = \{\phi^t \quad \phi^b\}$; $N_u = [N_{u1} \quad N_{u2} \quad N_{u3} \quad N_{u4}]$ and $N_\phi = [N_{\phi1} \quad N_{\phi2} \quad N_{\phi3} \quad N_{\phi4}]$ are matrix of shape functions with their components are shown below:

$$N_{ui} = [Nu_{i1} \; Nu_{i2} \; Nu_{i3} \; Nu_{i4}] \tag{8}$$

$$Nu_{i1} = \begin{Bmatrix} N_i \\ 0 \\ 0 \end{Bmatrix}; \; Nu_{i2} = \begin{Bmatrix} 0 \\ N_i \\ 0 \end{Bmatrix}$$

with

$$Nu_{i3} = \begin{bmatrix} -zH_{1i,x} & -zH_{2i,x} & -zH_{3i,x} \\ -zH_{1i,y} & -zH_{2i,y} & -zH_{3i,y} \\ H_{1i} & H_{2i} & H_{3i} \end{bmatrix};$$

$$Nu_{i4} = \begin{bmatrix} -\Re H_{1i,x} & -\Re H_{2i,x} & -\Re H_{3i,x} \\ -\Re H_{1i,y} & -\Re H_{2i,y} & -\Re H_{3i,y} \\ H_{1i} & H_{2i} & H_{3i} \end{bmatrix}.$$

$$N_{\Phi i} = \begin{bmatrix} Z^t N_i & 0 \\ 0 & Z^b N_i \end{bmatrix} \tag{9}$$

Therefore, the strain and electric fields can be expressed as:

$$\{\varepsilon\} = \nabla \bar{u} = \sum_{i=1}^{4} [B_{ui}]\{d_i\} = B_u d \tag{10}$$

$$\{E\} = -\text{grad}\bar{\Phi} = -\sum_{i=1}^{4} [B_{\phi i}]\{\Phi_i\} = B_\phi \Phi \tag{11}$$

where B_u and B_ϕ are defined as follows:

$$B_u = \sum_{i=1}^{4} [B_{u1} \; B_{u2} \; B_{u3}]$$

with

$$B_{u1} = \begin{bmatrix} N_{i,x} & 0 \\ 0 & N_{i,y} \\ N_{i,y} & N_{i,x} \\ 0 & 0 \\ 0 & 0 \end{bmatrix};$$

$$B_{u2} = \begin{bmatrix} -zH_{1i,xx} & -zH_{2i,xx} & -zH_{3i,xx} \\ -zH_{1i,yy} & -zH_{2i,yy} & -zH_{3i,yy} \\ -zH_{1i,xy} & -zH_{2i,xy} & -zH_{3i,xy} \\ 0 & 0 & 0 \\ 0 & 0 & 0 \end{bmatrix}; \tag{12}$$

$$B_{u3} = \begin{bmatrix} -\Re H_{1i,xx} & -\Re H_{2i,xx} & -\Re H_{3i,xx} \\ -\Re H_{1i,yy} & -\Re H_{2i,yy} & -\Re H_{3i,yy} \\ -\Re H_{1i,xy} & -\Re H_{2i,xy} & -\Re H_{3i,xy} \\ \Re_{,z} H_{1i,y} & \Re_{,z} H_{2i,y} & \Re_{,z} H_{3i,y} \\ \Re_{,z} H_{1i,x} & \Re_{,z} H_{2i,x} & \Re_{,z} H_{3i,x} \end{bmatrix}.$$

$$B_\phi = \sum_{i=1}^{4} [B_{\phi t} \; B_{\phi b}]^T$$

$$B_{\phi t} = \begin{bmatrix} Z^t_{p,x} & Z^t_{p,y} & Z^t_{p,z} \\ 0 & 0 & 0 \end{bmatrix}; \tag{13}$$

with

$$B_{\phi b} = \begin{bmatrix} 0 & 0 & 0 \\ Z^b_{p,x} & Z^b_{p,y} & Z^b_{p,z} \end{bmatrix}.$$

Hamilton's principle is used to establish the equilibrium equations of elements:

$$\int_{t_1}^{t_2} (\delta U_e - \delta K_e - \delta W_e)\, dt = 0 \tag{14}$$

where δU_e, δK_e and δW_e represent the variations of strain energy, kinetic energy, and external work,

respectively. They are defined as:

$$\delta U = \int_{\Omega} \left(\sigma \delta \varepsilon^{T} - D \delta E^{T} \right) d\Omega \quad (15)$$

$$\delta K = \int_{\Omega} \rho \ddot{\bar{u}} \delta \bar{u}^{T} d\Omega \quad (16)$$

The variation of external loading δW_e, under the effect in-plane load $N_x^0 = \lambda_x N_0$, and $N_y^0 = \lambda_y N_0$ is determined as follows:

$$\delta W_e = N_0 \int_{\Omega_e} \left(\lambda_x w_{,x} \delta w_{,x} + \lambda_y w_{,y} \delta w_{,y} \right) d\Omega \quad (17)$$

Substitute (5), (6) and (10) into (15), (16) and (17), then substitute into (14) and perform the transformation to get the equations of motion:

$$\begin{bmatrix} M_{uu} & 0 \\ 0 & 0 \end{bmatrix} \begin{Bmatrix} \ddot{d}_e \\ \ddot{\Phi}_e \end{Bmatrix} + \left(\begin{bmatrix} K_{uu} & K_{u\phi} \\ K_{\phi u} & K_{\phi\iota} \end{bmatrix} - N_0 \begin{bmatrix} K_{eg}^{uu} & 0 \\ 0 & 0 \end{bmatrix} \right) \begin{Bmatrix} d_e \\ \Phi_e \end{Bmatrix} = \begin{Bmatrix} 0 \\ 0 \end{Bmatrix} \quad (18)$$

The following equation is obtained after performing the mathematical transformation:

$$M_e \ddot{d}_e + \left(K_e - N_0 K_{eg} \right) d_e = 0 \quad (19)$$

in which:

$M_e = M_{uu} = \int_{\Omega} \rho N_u^{T} N_u d\Omega$ is element mass matrix.

$K_e = K_e^{uu} = \int_{\Omega} B_u^{T} \bar{C} B_u d\Omega$ is the element stiffness matrix at “closed circuit”.

$K_e = K_e^{uu} + K_{u\phi} K_{\phi\phi}^{-1} K_{u\phi}^{T}$ is the element stiffness matrix at “open circuit”.

where $K_{u\phi} = -\int_{\Omega} B_u^{T} e^{T} B_{\phi} d\Omega$ is the electromechanical element stiffness matrix, and $K_{\phi\phi} = \int_{\Omega} B_{\phi}^{T} p B_{\phi} d\Omega$ is the element electric stiffness matrix.

The implementation of element coupling yields the system of motion equations for a 2D-FGM plate integrated with piezoelectric layers subjected to in-plane loading as follows:

$$M\ddot{D} + \left(K - N_0 K_G \right) D = 0 \quad (20)$$

Finally, the free vibration frequency can be obtained by solving the equation:

$$\left| K - \omega^2 M \right| = 0 \quad (21)$$

The critical load is obtained by solving the equation:

$$\left| K - N_0 K_G \right| = 0 \quad (22)$$

4. Numerical results and disscussions

Building upon the developed finite element model, a Matlab-based computer program was established to calculate the natural frequencies and critical buckling loads of the 2DFGM-Pie plate. The materials used in the studies include PZT-4, Al, and Al_2O_3. These materials have the following properties: PZT-4 [3]: $C_{11} = C_{22} = 132$ GPa, $C_{12} = 71$ GPa, $C_{33} = 115$ GPa, $C_{13} = 73$ GPa, $C_{55} = 26$ GPa, $e_{31} = -4.1$ Cm^{-2}, $e_{33} = 14.1$ Cm^{-2}, $e_{15} = 10,5$ C m^{-2}, $p_{11} = 7.124$ nF m^{-1}, $p_{33} = 5.841$ nF m^{-1}, $\rho =$ 7500 kg m^{-3}; Al [3]: $\rho_m = 2707$ (kg m^{-3}), $E_m = 70$ GPa, $\nu_m = 0,3$; Al_2O_3 [3]: $\rho_c = 3800$ kg m^{-3}, $E_c = 380$ GPa, $\nu_c = 0,3$.

The dimensionless formulas employed in this study are:

$$\bar{N}_{cr} = \frac{a^2 N_{cr}}{100 E_0 h^3} \quad (E_0 = 1\text{GPa}) \quad (23)$$

4.1. Comparative studies

This section presents two verification examples to evaluate the accuracy and convergence characteristics of the proposed model. In the first example, the results are compared with the analytical solution of a sandwich plate with a piezoelectric surface layer and an FGM core whose material properties vary through the thickness [3]. The comparison of the plate’s dimensionless natural frequencies is summarized in Table 1.

The second validation example evaluates the dimensionless critical load $\hat{N}_{cr} = N_{cr} \left(a^2 / \left(\pi^2 D_0 \right) \right)$, $D_0 = 12 \left(1 - \nu^2 \right) / h^2$ of an isotropic square plate. The results are compared with the reference values reported by Uymaz and Aydogdu [18-20], obtained using a three-dimensional model, as summarized in Table 2.

Table 1. Comparison of natural frequencies f (Hz) for a sandwich plate with an FGM core (Al_2O_3) and a piezoelectric surface layer (h_c = 0.05m, a = b = 10h_c)

Model	BC's	Electrical boundary	h_p/h_c = 0.1		h_p/h_c = 0.2	
			p_z			
			0.5	2	0.5	2
FSDT [3]	SSSS	Clocc	715.319	613.305	715.319	620.355
		Opcc	731.920	634.772	731.920	655.648
Present		Clocc	727.391	644.874	706.385	642.306
		Opcc	743.654	664.533	735.712	675.551
FSDT [3]	SCSC	Clocc	998.185	853.554	964.112	852.529
		Opcc	1019.895	881.128	1003.245	897.511
Present		Clocc	1021.249	872.799	991.983	877.895
		Opcc	1044.046	901.656	1032.167	924.457

Table 2. Comparison of critical loads $\hat{N}_{cr}$ for an isotropic square plate under a uniform load along the *x*-direction

a/h	3D [18]	3D [19]	3D [20]	Present
20	3.931	3.911	3.9499	3.9283
100	4.020	4.022	3.9899	3.9812

Detailed comparisons in Tables 1 and 2 indicate that the discrepancy between the results obtained from the present model and those reported by other authors is negligible. This confirms the high accuracy of the developed model and computer program, providing a reliable basis for further investigations. In addition, a convergence study was performed, and a 16×16 element mesh was found to be sufficient. This mesh is therefore adopted for all subsequent numerical analyses.

4.2. Parametric studies

4.2.1. Buckling analysis

In this section, a study on the dimensionless critical buckling load $\bar{N}_{cr}$ is presented for a rectangular 2D-FGM/Pie sandwich plate with dimensions a×b×h. The plate is under uniform biaxial compression and is composed of a 2D-FGM core and two PZT-4 piezoelectric face sheets.

The influence of the volume fraction indices p_x and p_z on the critical buckling load of a 2D-FGM/Pie plate under uniform biaxial compression along the x and y directions is detailed in Table 3. The study was performed considering four types of mechanical boundary conditions (SSSS, CCCC, SCSC, SFSF) and two electrical boundary conditions (Clocc and Opcc). The results indicate that as the indices p_x and p_z increase, the plate's critical load decreases. This trend arises because increasing these indices reduces the volume fraction of the ceramic component (Al_2O_3) while increasing that of the metallic component (Al). Since the elastic modulus of Al_2O_3 is much higher than that of Al, a lower ceramic-to-metal ratio reduces the overall stiffness of the plate, thereby lowering its critical buckling load and, consequently, its compressive load-bearing capacity.

Fig. 2 shows the influence of the geometric ratio b/a and the core length-to-thickness ratio a/h_c on the dimensionless critical buckling load of a 2D-FGM/Pie plate under uniform biaxial compression (with a = 1 m fixed). The results reveal two contrasting trends: as b/a increases, the dimensionless critical buckling load decreases, whereas as a/h_c increases, it increases for all investigated electrical and mechanical boundary

conditions. This behavior is attributed to changes in bending stiffness associated with geometric ratios. An increase in a/h_c makes the plate more slender but enhances its bending stiffness, improving its resistance to global instability. In contrast, an increase in b/a raises the plate's slenderness in the transverse direction, thereby reducing its ultimate compressive load-bearing capacity.

Fig. 3 shows that the critical buckling load $\bar{N}_{cr}$ of the 2D-FGM/Pie plate in the Opcc case is consistently higher than in the Clocc case. This behavior can be explained by the inverse piezoelectric effect. When the circuit is open, the generated electrical energy is not dissipated but is converted into mechanical energy, which increases the effective stiffness of the structure and, consequently, the critical buckling load. In contrast, in a closed circuit, the electrical potential is nullified due to grounding, preventing electro-mechanical energy conversion. As a result, the plate's stiffness is not enhanced, and its critical buckling load remains lower.

Table 3. Dimensionless critical buckling load $\bar{N}_{cr}$ of a 2D-FGM/Pie plate under uniform biaxial compression ($a = b = 1m$, $h_c = 0.1a$, $h_p = 0.1h_c$)

p_z	p_x	SSSS		CCCC		SCSC		SFSF	
		Clocc	Opcc	Clocc	Opcc	Clocc	Opcc	Clocc	Opcc
0	0	4.279	4.418	10.319	10.632	7.768	8.011	2.078	2.120
	0.5	3.847	3.986	9.270	9.583	6.970	7.213	1.873	1.915
	1	3.476	3.615	8.356	8.670	6.257	6.501	1.694	1.736
	5	1.994	2.139	4.626	4.942	3.373	3.621	0.949	0.994
	10	1.574	1.715	3.560	3.857	2.642	2.879	0.723	0.769
0.5	0	3.104	3.244	7.302	7.624	5.494	5.743	1.522	1.563
	0.5	2.842	2.982	6.698	7.019	5.038	5.285	1.395	1.436
	1	2.618	2.758	6.176	6.495	4.634	4.881	1.284	1.326
	5	1.727	1.868	4.018	4.324	2.975	3.217	0.828	0.871
	10	1.459	1.596	3.340	3.631	2.505	2.738	0.683	0.727
1	0	2.626	2.767	5.942	6.269	4.483	4.735	1.307	1.347
	0.5	2.436	2.576	5.548	5.872	4.184	4.434	1.210	1.251
	1	2.273	2.413	5.206	5.527	3.920	4.168	1.127	1.168
	5	1.614	1.753	3.734	4.035	2.791	3.028	0.779	0.821
	10	1.407	1.543	3.230	3.518	2.437	2.667	0.666	0.709
5	0	1.925	2.059	4.148	4.439	3.183	3.415	0.978	1.017
	0.5	1.836	1.968	4.007	4.295	3.070	3.300	0.928	0.967
	1	1.758	1.890	3.879	4.164	2.968	3.196	0.885	0.924
	5	1.432	1.564	3.273	3.551	2.490	2.714	0.700	0.740
	10	1.321	1.454	3.041	3.318	2.313	2.536	0.637	0.677
10	0	1.694	1.824	3.731	4.002	2.873	3.092	0.853	0.892
	0.5	1.633	1.762	3.631	3.901	2.792	3.010	0.820	0.858
	1	1.580	1.710	3.541	3.812	2.719	2.937	0.791	0.829
	5	1.363	1.494	3.133	3.406	2.389	2.609	0.667	0.707
	10	1.288	1.420	2.979	3.254	2.268	2.489	0.624	0.664

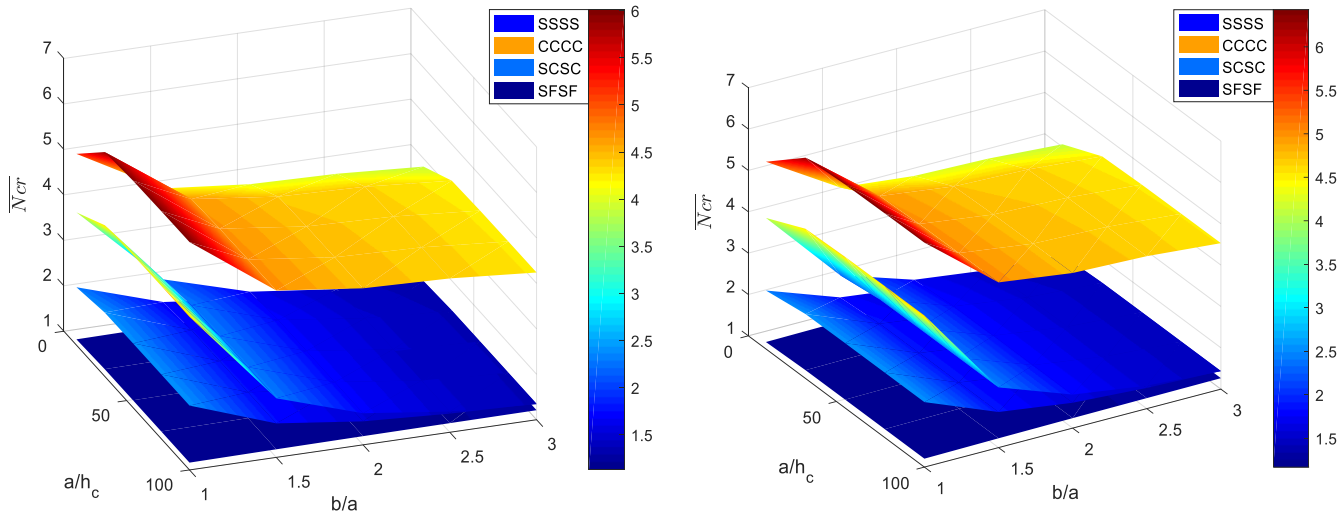

(a) Clocc (b) Opcc

Fig. 2. Effect of the ratios a/h_c and b/a on the dimensionless critical buckling load $\left(\bar{N}_{cr}\right)$ of a 2D-FGM/Pie plate ($a = 1m$, $h_p = 0.1h_c$).

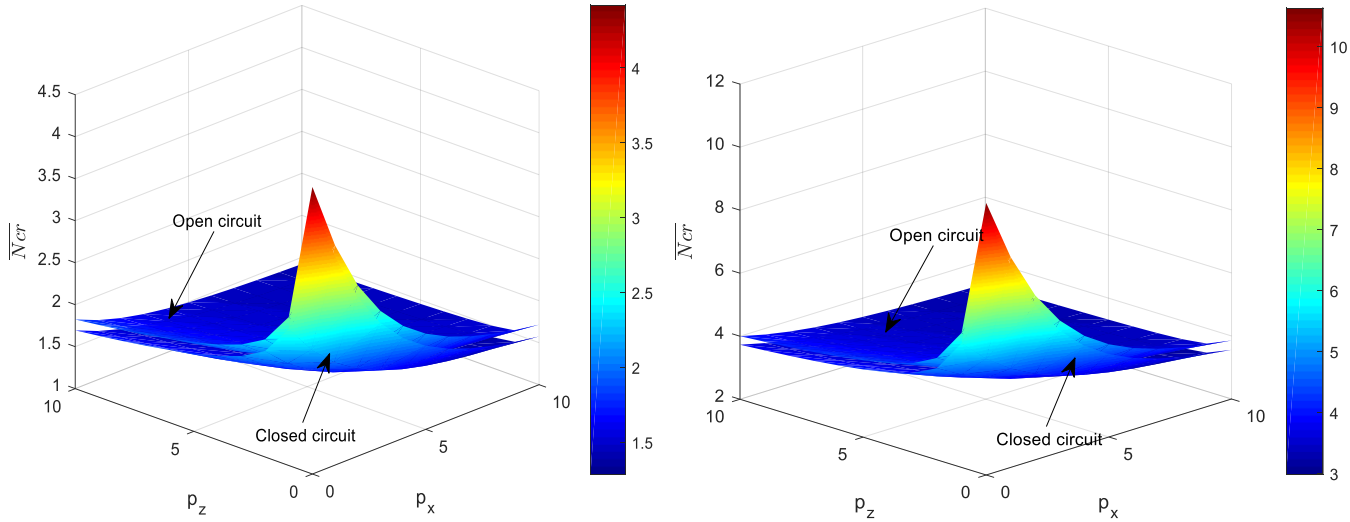

(a) SSSS (b) CCCC

Fig. 3. Effect of electrical boundary conditions on the dimensionless critical buckling load $\left(\bar{N}_{cr}\right)$ of a 2D-FGM/Pie plate ($a = b = 1m$, $h_c = 0.1a$, $h_p = 0.1h_c$).

Fig. 4 illustrates the influence of the thickness ratio h_p/h_c on the critical buckling load of a 2D-FGM/Pie plate. In this analysis, the geometric parameters of the plate are kept constant ($a \times b \times h$ = 1×1×0.1 m). The results reveal two contrasting trends depending on the electrical boundary condition: In the closed-circuit case, as the ratio h_p/h_c increases, the plate's critical buckling load tends to decrease. Conversely, in the open-circuit state (at p_z = 1, p_x = 10), the critical buckling load tends to increase as the ratio h_p/h_c rises. This difference reflects the role of the inverse piezoelectric effect in enhancing stiffness. The open circuit allows electrical energy to be converted into mechanical energy, which increases the effective stiffness and load-bearing capacity of the plate. Therefore, the impact of the piezoelectric layer on structural stability is strongly dependent on the electrical boundary conditions.

Fig. 5 illustrates the influence of four types of mechanical boundary conditions (SSSS, CCCC,

SCSC, and SFSF) on the dimensionless critical buckling load $\left(\bar{N}_{cr}\right)$ of the 2D-FGM/Pie plate as the volume fraction indices p_x and p_z vary. The results indicate that the plate's dimensionless critical buckling load is directly related to the degree of restraint imposed by its boundary conditions. Specifically, a plate with four clamped edges (CCCC) exhibits the highest dimensionless critical buckling load, followed by SCSC, SSSS, and the lowest is SFSF. This behavior can be physically explained by the fact that the higher the boundary restraint, the more the plate's displacement and deformation are restricted, which increases the overall stiffness of the structure and, consequently, the plate's critical buckling load.

4.2.2. Free vibration analysis

This section presents a numerical example to investigate the natural frequencies of a rectangular sandwich plate with dimensions $a \times b \times h$. The plate consists of a 2D-FGM core and two face sheets made of PZT-4 piezoelectric material.

In the first example, the influence of the volume fraction indices p_x and p_z on the fundamental natural frequency f (Hz), of a 2D-FGM/PZT plate, as summarized in Table 4 and illustrated in Fig. 6. Four mechanical boundary condition types (SSSS, CCCC, SCSC, and SFSF), together with two electrical conditions (closed- and open-circuit), are taken into account. The results show that as p_x and p_z increase from 0, 0.5, 1, 2, 5 to 10, the fundamental frequency gradually decreases, indicating a significant influence of these indices on the overall stiffness of the plate. This trend is consistent with the buckling analysis: higher values of these indices reduce the overall stiffness of the plate, which consequently lowers its fundamental natural frequency.

The influence of the geometric ratios b/a and the core length-to-thickness ratio a/h_c on the fundamental natural frequency f (Hz) of the 2D-FGM/Pie plate is illustrated in Fig. 7 (with side a = 1 m fixed). The results show that, with a fixed side length a, an increase in the b/a ratio causes the fundamental frequency to decrease. Similarly, for all considered mechanical and electrical boundary conditions, the frequency f (Hz) decreases as the a/h_c ratio increases (i.e., the plate becomes more slender). This behavior can be attributed to the fact that a higher a/h_c ratio makes the plate more flexible, thereby reducing its bending stiffness. The lower stiffness diminishes the plate's resistance to deformation, leading to a decrease in its vibration frequency.

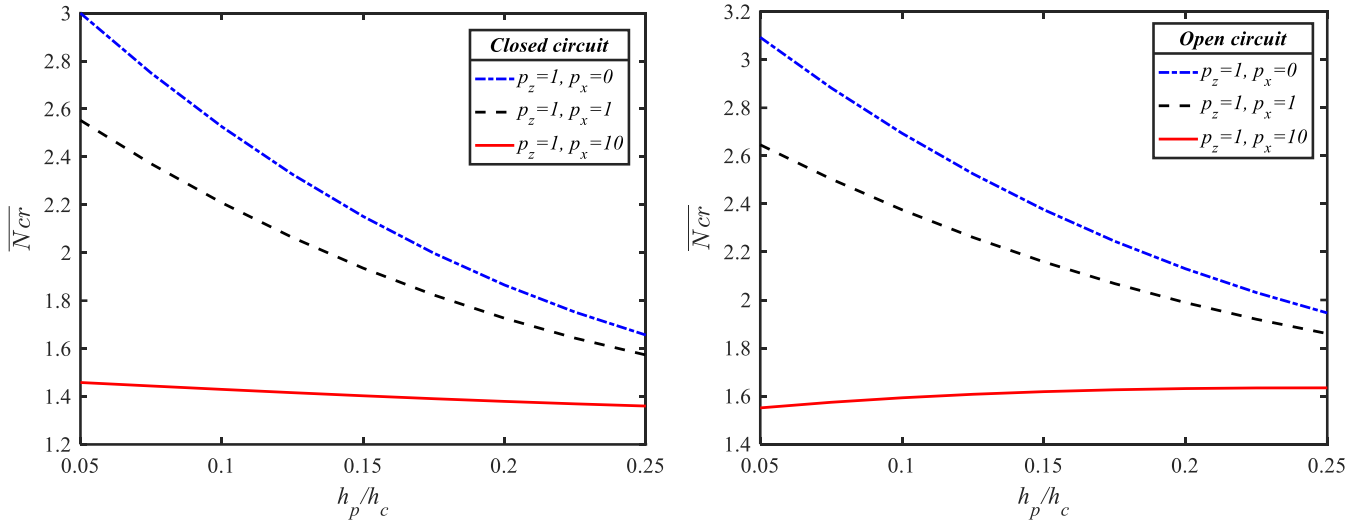

(a) SSSS, Clocc (b) SSSS, Opcc

Fig. 4. Effect of the ratio h_p/h_c on the dimensionless critical buckling load $\bar{N}_{cr}$ of a 2D-FGM/Pie plate (a = b = 1m, h_c = 0.1a).

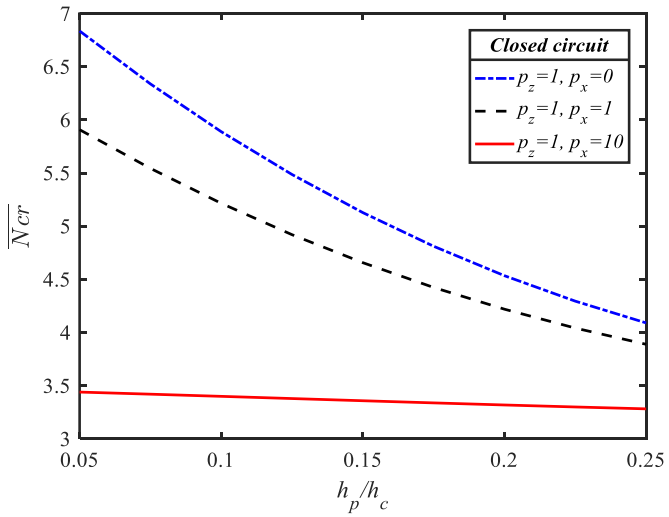

(c) CCCC, Clocc

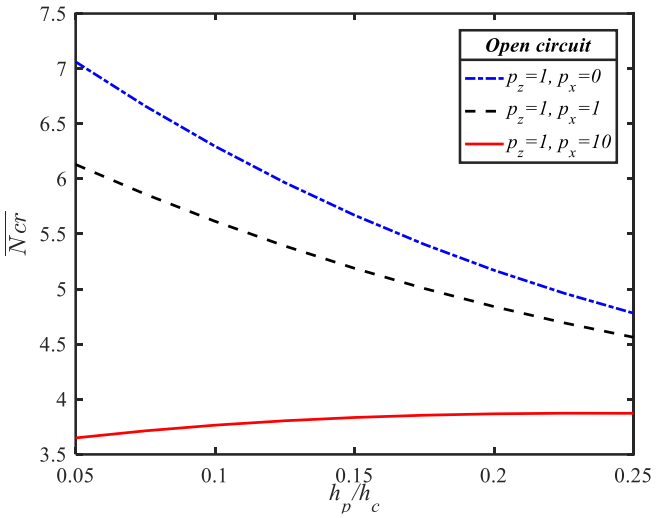

(d) CCCC, Opcc

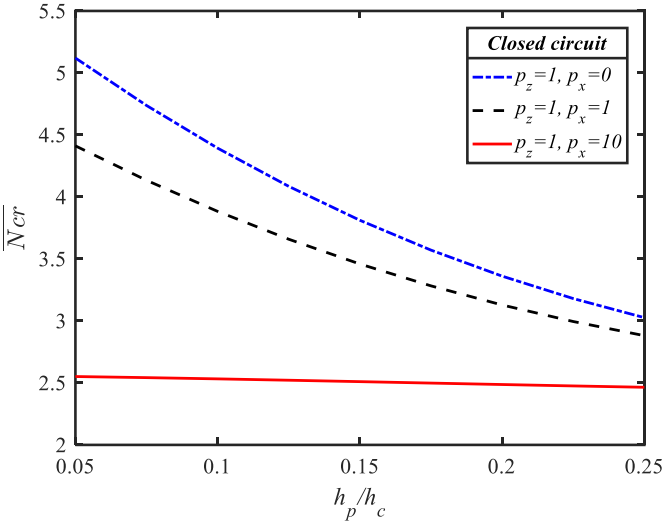

(e) SCSC, Clocc

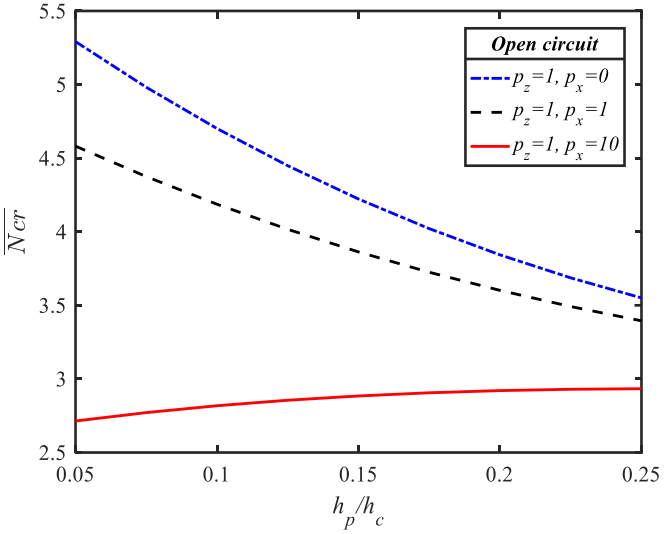

(f) SCSC, Opcc

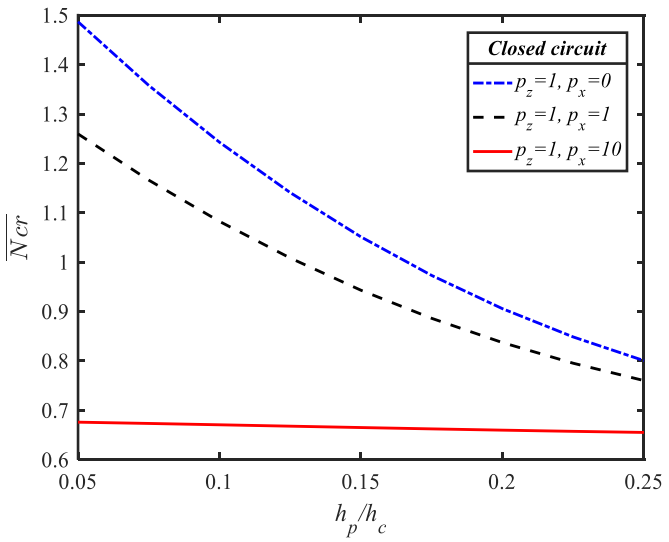

(g) SFSF, Clocc

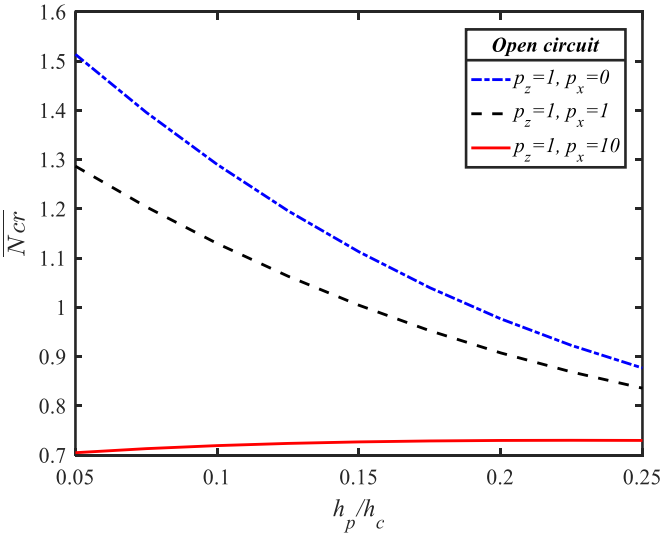

(h) SFSF, Opcc

Fig. 4. (continued)

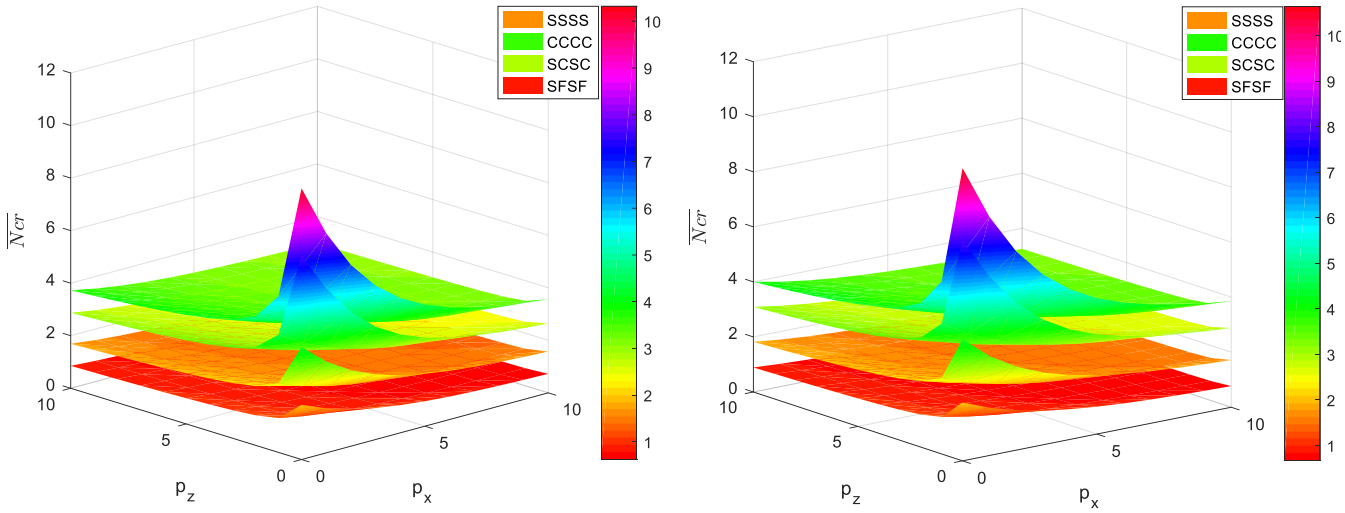

(a) Clocc (b) Opcc

Fig 5. Effect of mechanical boundary conditions on the dimensionless critical buckling load $\bar{N}_{cr}$ of a 2D-FGM/Pie plate (a = b = 1m, h_c = 0.1a, h_p = 0.1h_c).

Table 4. Fundamental natural frequency f (Hz) of a 2D-FGM/PZT plate (a = b = 1m, h_c = 0.1a, h_p = 0.1h_c)

p_z	p_x	SSSS		CCCC		SCSC		SFSF	
		Clocc	Opcc	Clocc	Opcc	Clocc	Opcc	Clocc	Opcc
0	0	824.60	837.91	1417.50	1438.63	1172.46	1190.59	412.86	417.89
	0.5	793.52	807.73	1362.88	1385.43	1128.24	1147.57	397.65	403.01
	1	764.85	780.00	1312.34	1336.37	1086.88	1107.47	383.17	388.89
	5	620.59	641.86	1056.86	1090.30	870.05	899.03	304.45	312.80
	10	560.98	584.92	950.94	987.93	778.23	810.87	270.37	280.05
0.5	0	727.39	743.65	1235.58	1262.28	1021.25	1044.05	365.98	372.07
	0.5	703.38	720.49	1195.31	1223.26	988.66	1012.54	353.98	360.39
	1	681.73	699.69	1158.95	1188.12	958.90	983.84	342.85	349.57
	5	579.45	602.14	985.04	1020.60	812.07	843.01	286.49	295.26
	10	538.92	563.49	914.35	952.04	751.38	784.70	263.44	273.15
1	0	681.79	699.84	1135.40	1165.94	939.58	965.62	345.58	352.29
	0.5	661.94	680.73	1105.53	1136.99	915.25	942.12	335.25	342.24
	1	644.18	663.68	1078.70	1111.01	893.18	920.84	325.77	333.03
	5	561.58	584.93	949.72	986.22	784.69	816.54	279.15	288.10
	10	529.18	554.04	895.92	933.88	738.64	772.22	260.53	270.25
5	0	607.60	628.34	983.31	1016.81	822.56	851.97	311.01	318.82
	0.5	594.96	616.15	969.13	1002.85	810.32	839.99	303.84	311.82
	1	583.71	605.35	956.07	990.07	799.07	829.03	297.39	305.55
	5	532.89	557.01	891.25	927.58	742.19	774.38	267.24	276.46
	10	513.50	538.65	864.22	901.81	717.32	750.76	255.59	265.28
10	0	575.44	597.12	940.67	973.74	789.11	818.52	293.28	301.51
	0.5	565.79	587.91	929.54	963.02	779.20	808.98	287.88	296.26
	1	557.37	579.89	919.51	953.41	770.27	800.43	283.10	291.64
	5	520.81	545.36	872.66	909.14	727.55	759.99	261.50	270.86
	10	507.19	532.55	854.15	891.81	709.87	743.40	253.32	263.02

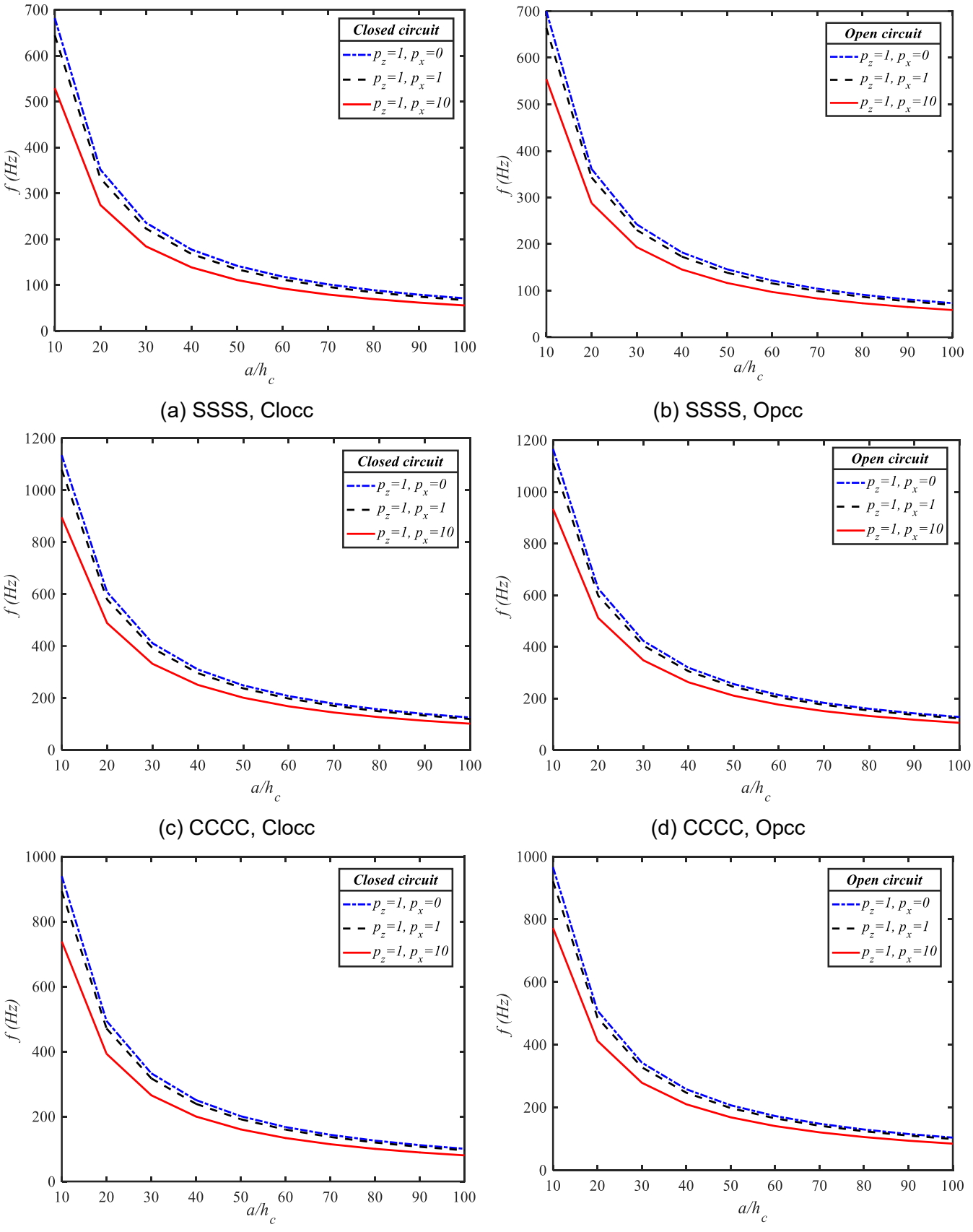

(a) SSSS, Clocc (b) SSSS, Opcc

(c) CCCC, Clocc (d) CCCC, Opcc

(e) SCSC, Clocc (f) SCSC, Opcc

Fig. 6. Effect of volume fraction indices p_x and p_z on the fundamental natural frequency f (Hz) of a 2D-FGM/PZT plate (a = b = 1m, $h_p = 0.1h_c$).

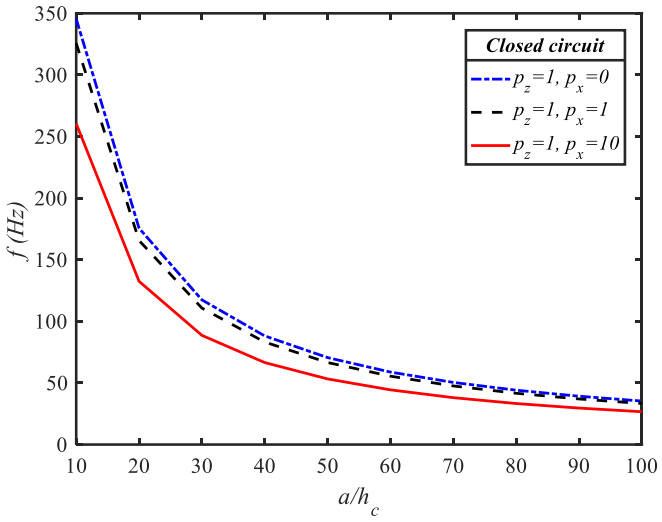

(g) SFSF, Clocc

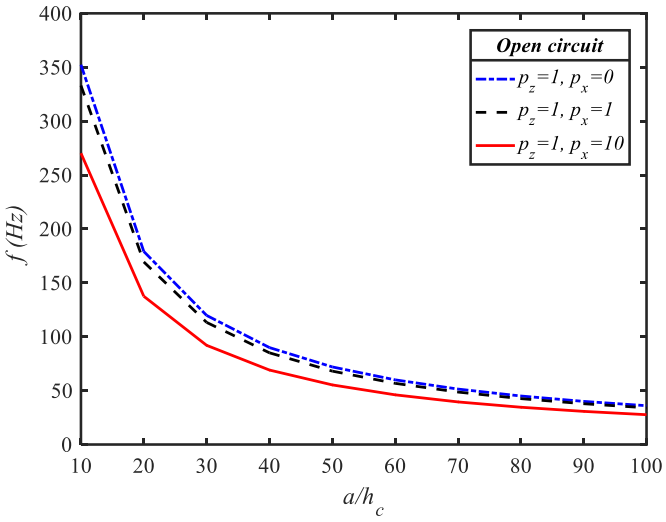

(h) SFSF, Opcc

Fig. 6. (continued)

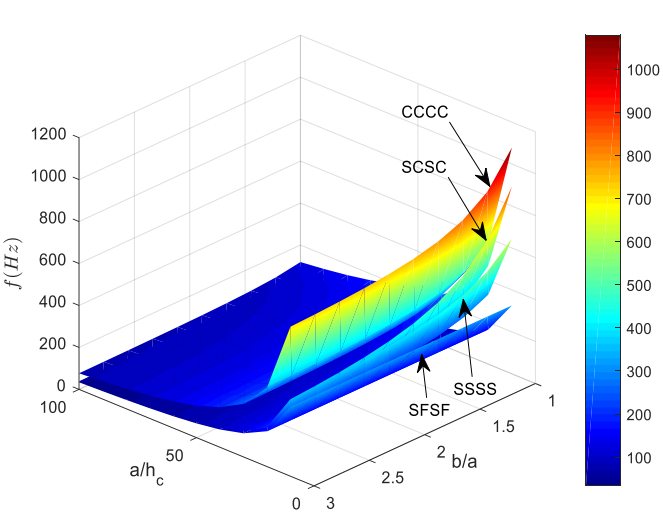

(a) Clocc

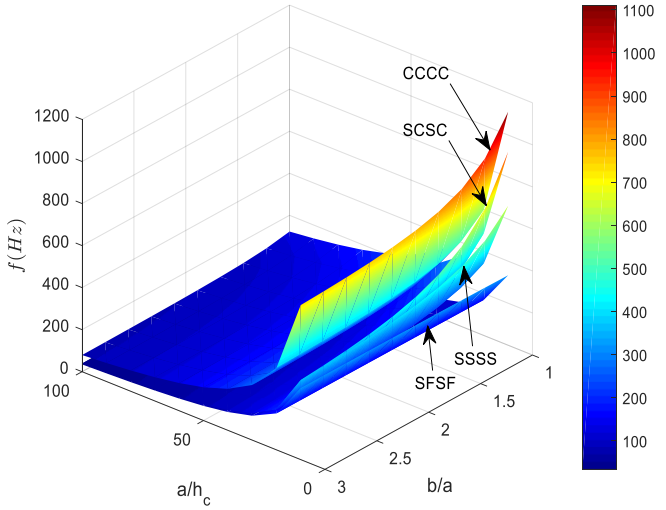

(b) Opcc

Fig. 7. Fundamental natural frequency of a 2D-FGM/Pie plate versus the ratios a/h and b/a (a = 1m).

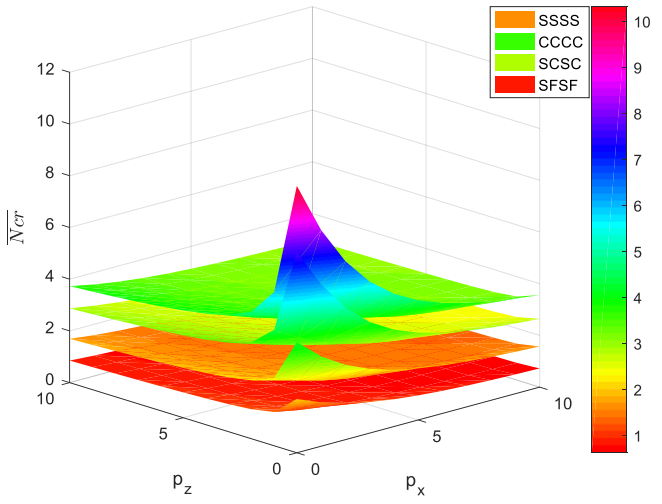

(a) SSSS

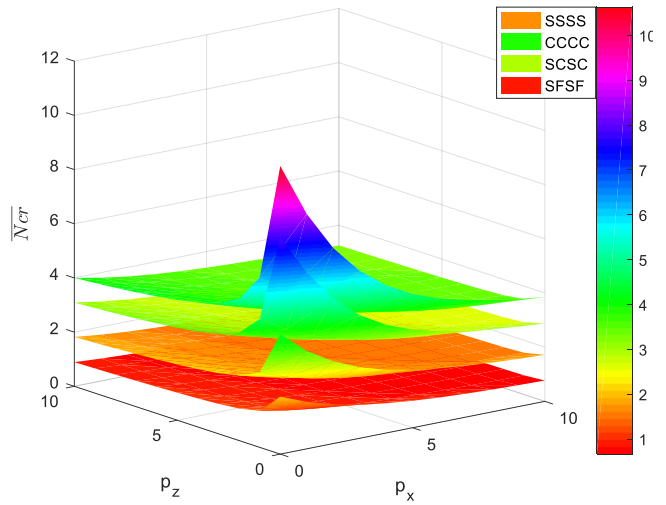

(b) CCCC

Fig. 8. Effect of electrical boundary conditions on the fundamental natural frequency f (Hz) of the 2D-FGM/Pie plate (a = b = 1m, a/h=10).

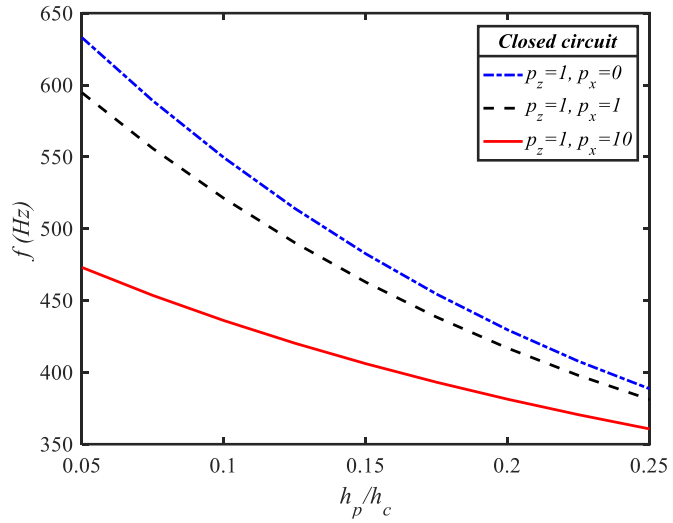

(a) SSSS, Clocc

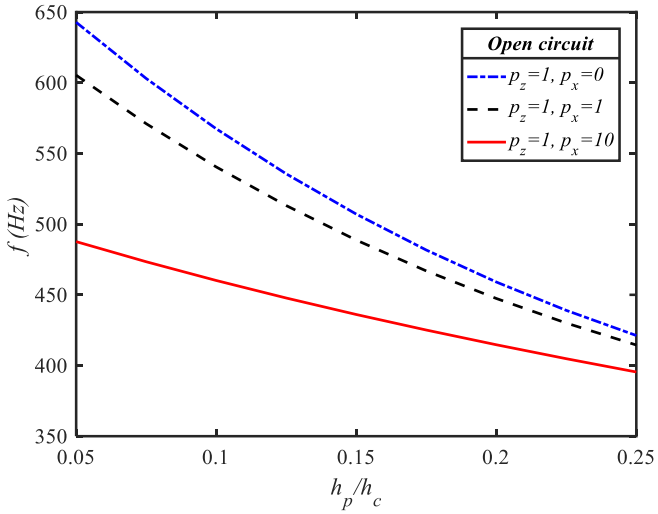

(b) SSSS, Opcc

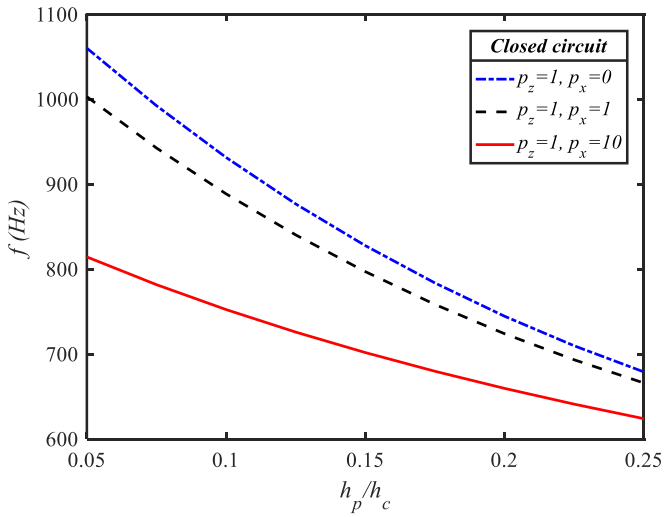

(c) CCCC, Clocc

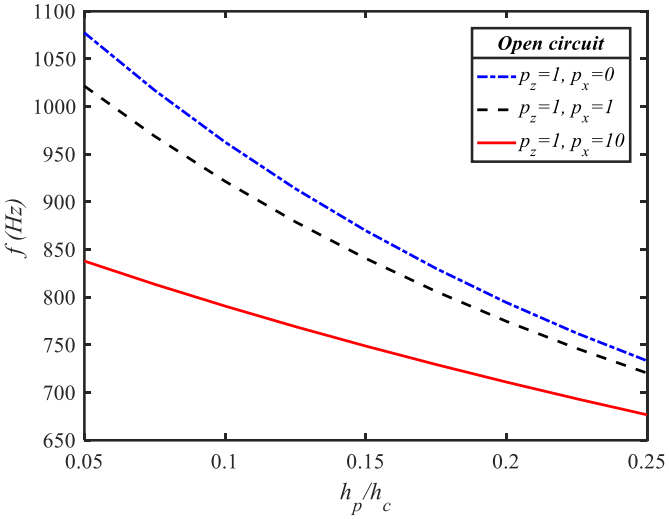

(d) CCCC, Opcc

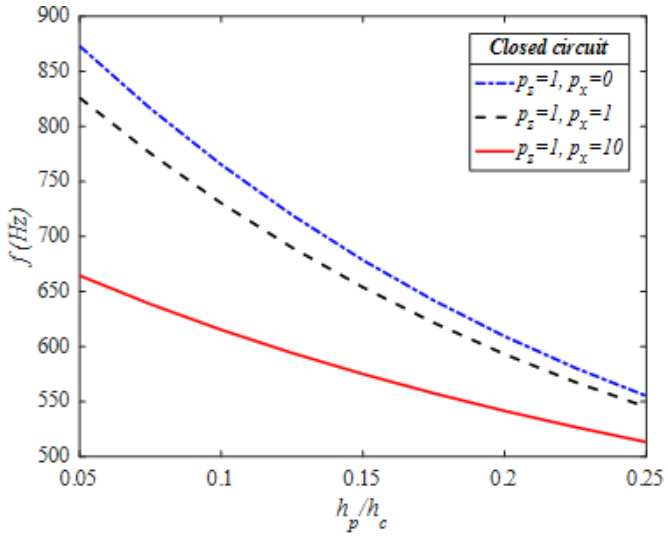

(e) SCSC, Clocc

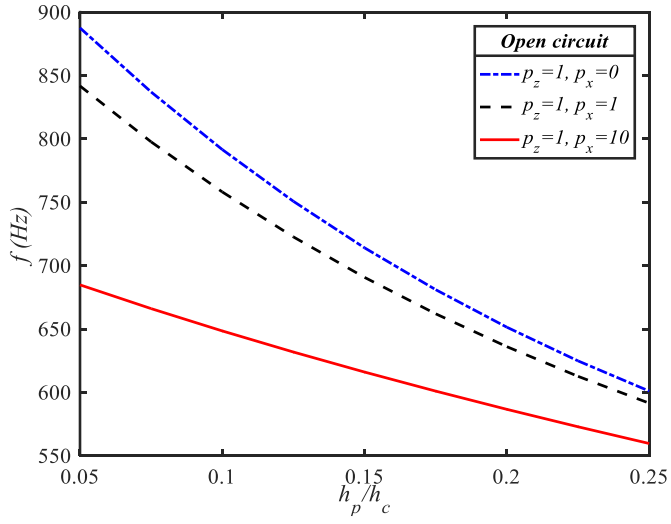

(f) SCSC, Opcc

Fig. 9. Effect of the ratio h_p/h_c on the fundamental natural frequency, f (Hz), of the 2D-FGM/Pie plate (a = b = 1m, a/h_c=10, $h_p = 0.1h_c$).

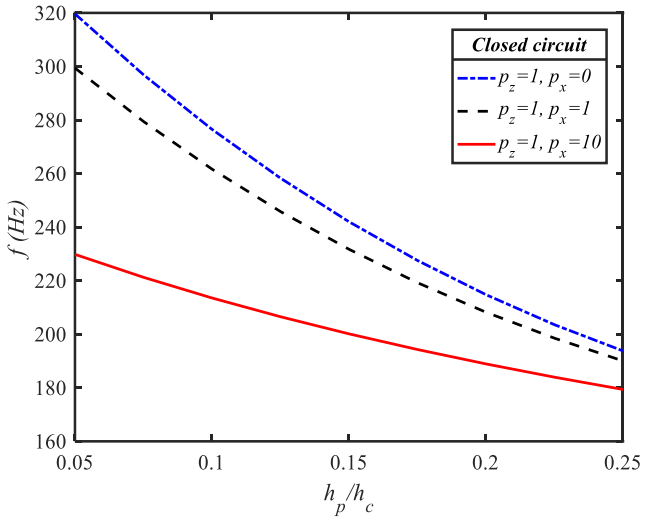

(g) SFSF, Clocc

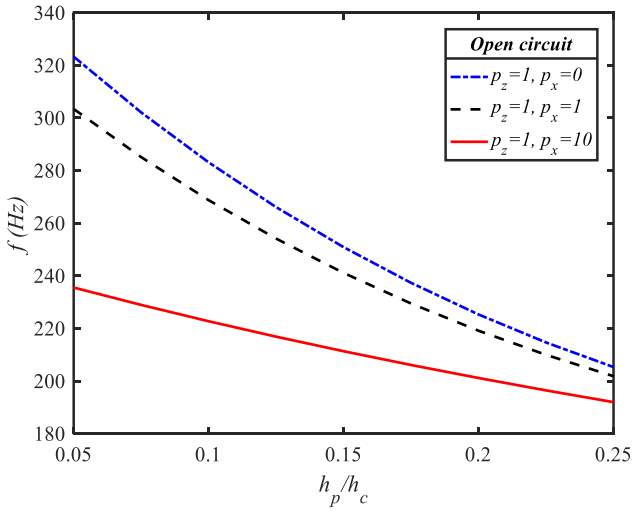

(h) SFSF, Opcc

Fig. 9. (continued)

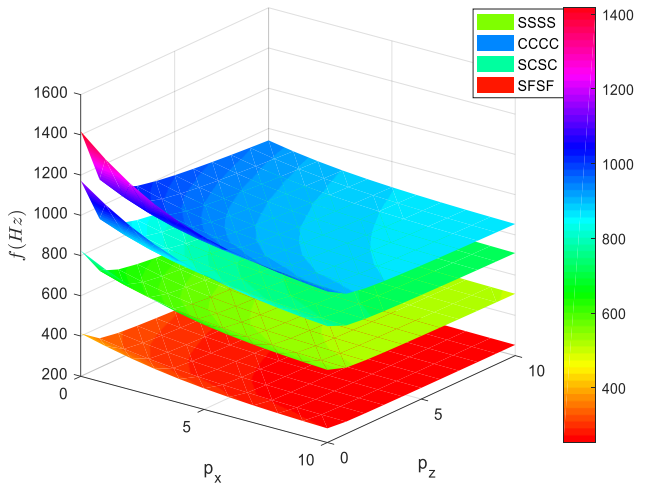

(a) Clocc

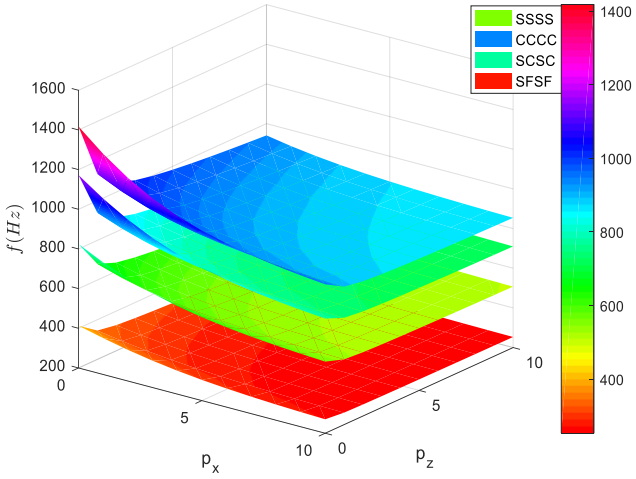

(b) Opcc

Fig. 10. Effect of mechanical boundary conditions on the natural frequency f (Hz) of the 2D-FGM/Pie plate (a = b = 1m, a/h_c=10, h_p = 0.1h_c).

Fig. 8 illustrates the influence of the two electrical boundary conditions of the piezoelectric layer (Clocc and Opcc) on the fundamental natural frequency f(Hz) of the plate as the volume fraction indices p_x and p_z vary. The results show that the natural frequency in the Opcc case is consistently higher than in the Clocc case. This trend is in agreement with the buckling analysis and further confirms that, under the Opcc condition, the piezoelectric effect enhances the effective stiffness of the structure, leading to higher critical buckling loads and vibration frequencies.

The influence of the thickness ratio h_p/h_c on the natural frequency f(Hz) of the 2D-FGM/Pie plate is presented in Fig. 9. The geometric parameters of the plate are kept constant ($a \times b \times h$ = 1×1×0.1 m), where the thickness of the piezoelectric layer (h_p) and the 2D-FGM core (h_c) change according to this ratio. The results indicate that the vibration frequency decreases as the ratio h_p/h_c increases. This is explained by the change in the plate's compositional makeup. As h_p increases, h_c decreases, while the 2D-FGM material has a significantly greater stiffness than the piezoelectric material. Therefore, increasing

the proportion of the softer material (the piezoelectric layer) and decreasing the proportion of the stiffer material (the 2D-FGM core) leads to a reduction in the overall stiffness of the plate, which in turn decreases its fundamental natural frequency.

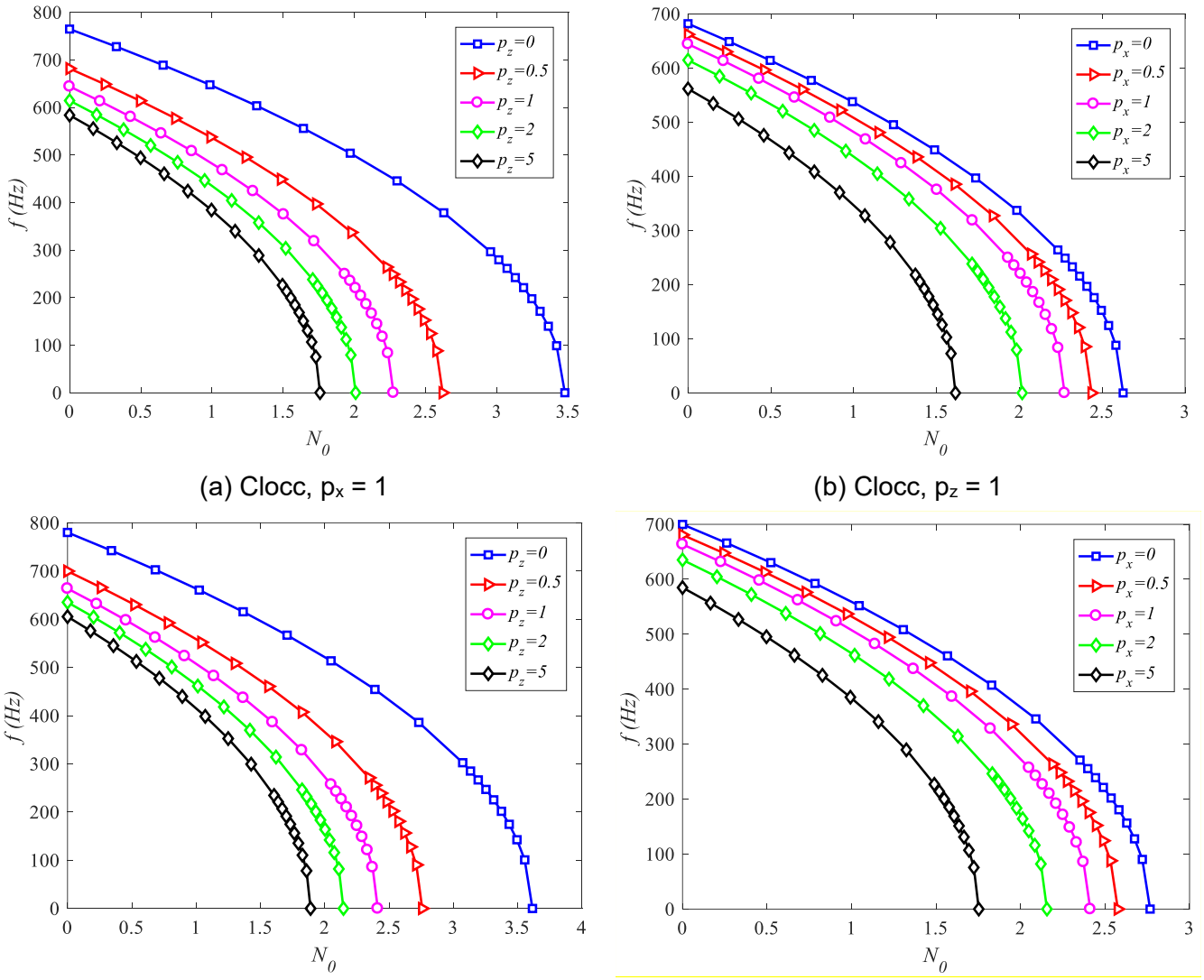

(a) Clocc, p_x = 1 (b) Clocc, p_z = 1

(c) Opcc, p_x = 1 (d) Opcc, p_z = 1

Fig. 11. Effect of volume fraction indexes p_x and p_z on the natural frequency f (Hz) with in-plane load Γ of the 2D-FGM/Pie plate (a = b = 1m, a/h_c=10, $h_p = 0.1h_c$, SSSS).

Fig. 10 indicates that the natural frequency f(Hz) of the 2D-FGM/Pie plate follows a trend similar to that observed in Fig. 2. Specifically, plates with a higher degree of boundary restraint (in the order CCCC > SCSC > SSSS > SFSF) exhibit greater overall stiffness, which consequently results in higher natural frequencies.

Fig. 11 illustrates the variation of the natural frequency f (Hz) of 2D-FGM/Pie plates with respect to the in-plane load N_0 for different values of the volume fraction indices p_x and p_z. When p_x = 1 and p_z increases from 0 to 5, the frequency decreases as N_0 increases, and the rate of decrease is higher for plates with larger p_z. Similarly, when p_z = 1 and p_x increases from 0 to 5, the frequency also decreases with increasing load Γ, and plates with larger p_x exhibit a faster reduction in frequency. Moreover, within the investigated range, the rate of frequency reduction due to an increase in p_x (with p_z fixed) is greater than that caused by an increase in p_z (with p_x fixed). This phenomenon is attributed to the fact that the in-plane compressive loading

reduces the effective stiffness of the plate, resulting in a corresponding decrease in the natural vibration frequency. The critical state of buckling instability occurs when the compressive load reaches its critical value, which mathematically corresponds to the point where the plate's natural vibration frequency becomes zero.

5. Conclusions

This study developed a finite element model based on the high-order shear deformation refined plate theory and four-node rectangular element to analyze the vibration and stability of a 2D-FGM plate with two integrated piezoelectric layers on the top and bottom surfaces. From the results, some conclusions are drawn as follows:

The volume fraction indices in both the length and thickness directions have a significant influence on the stiffness of the plate. Specifically, as these indices increase, the ceramic content decreases and the metal content increases, leading to a decrease in the stiffness of the plate and as a result, both the natural vibration frequency and the critical force of the plate decrease.

The influence of the piezoelectric effect is evidenced by the difference between the two electrical boundary conditions. Both the natural frequency and the critical buckling load are consistently higher in the open-circuit state than in the closed-circuit state, as electrical energy is converted into mechanical energy, thereby enhancing the effective stiffness of the plate.

The effect of the thickness ratio h_p/h_c on the natural frequency and critical buckling load is dependent on the electrical boundary condition, which highlights the complex electro-mechanical interaction in the piezoelectric layers.

The effective stiffness and oscillation frequency of the plate are observed to decrease under compression. Notably, these values become zero when the compressive force reaches the critical buckling force.

These findings not only provide a deeper understanding of the vibration and buckling behavior of 2D-FGM/Pie plates but also offer a useful reference for the design and optimization of smart structures utilizing FGM and piezoelectric materials.

Acknowledgements

This research is funded by Vietnam National Foundation for Science and Technology Development (NAFOSTED) under grant number 107.02-2023.20.

References

[1] N.T.B. Lieu, N.X. Hung. (2019). Static analysis of piezoelectric functionally graded porous plates reinforced by graphene platelets. *Journal of Science and Technology in Civil Engineering (STCE)-NUCE*, 13(3), 58-72. https://doi.org/10.31814/stce.nuce2019-13(3)-06

[2] J. Rouzegar, F. Abad. (2015). Free vibration analysis of FG plate with piezoelectric layers using four-variable refined plate theory. *Thin-Walled Structures*, 89, 76-83. https://doi.org/10.1016/j.tws.2014.12.010

[3] M.A.A. Farsangi, A.R. Saidi. (2012). Levy type solution for free vibration analysis of functionally graded rectangular plates with piezoelectric layers. *Smart Materials and Structures*, 21(9), 094017. DOI 10.1088/0964-1726/21/9/094017

[4] Z. Zhong, T. Yu. (2006). Vibration of a simply supported functionally graded piezoelectric rectangular plate. *Smart Materials and Structures*, 15(5), 1404. DOI 10.1088/0964-1726/15/5/029

[5] F. Abad, J. Rouzegar. (2017). An exact spectral element method for free vibration analysis of FG plate integrated with piezoelectric layers. *Composite Structures*, 180, 696-708. https://doi.org/10.1016/j.compstruct.2017.08.030

[6] B. Behjat, M. Salehi, M. Sadighi, A. Armin, M. Abbasi. (2009). Static, dynamic, and free vibration analysis of functionally graded piezoelectric panels using finite element

method. *Journal of Intelligent Material Systems and Structures*, 20(13), 1635-1646. https://doi.org/10.1177/1045389X09104113

[7] S.Q. Zhang, Y.S. Gao, G.Z. Zhao, Y.J. Yu, M. Chen, X.F. Wang. (2020). Geometrically nonlinear analysis of CNT-reinforced functionally graded composite plates integrated with piezoelectric layers. *Composite Structures*, 234, 111694. https://doi.org/10.1016/j.compstruct.2019.111694

[8] J. Rouzegar, M. Davoudi. (2020). Forced vibration of smart laminated viscoelastic plates by RPT finite element approach. *Acta Mechanica Sinica*, 36, 933-949. https://doi.org/10.1007/s10409-020-00964-1

[9] A. Aghakhani, P.L. Motlagh, B. Bediz, I. Basdogan. (2019). A general electromechanical model for plates with integrated piezo-patches using spectral-Tchebychev method. *Journal of Sound and Vibration*, 458, 74-88. https://doi.org/10.1016/j.jsv.2019.06.016

[10] P.L. Motlagh, M.R. Anamagh, B. Bediz, I. Basdogan. (2021). Electromechanical analysis of functionally graded panels with surface-integrated piezo-patches for optimal energy harvesting. *Composite Structures*, 263, 113714.https://doi.org/10.1016/j.compstruct.2021.113714

[11] T.V. Do, D.K. Nguyen, N.D. Duc, D.H. Doan, T.Q. Bui (2017). Analysis of bi-directional functionally graded plates by FEM and a new third-order shear deformation plate theory. *Thin-Walled Structures*, 119, 687-699. https://doi.org/10.1016/j.tws.2017.07.022

[12] A. Harsha, P. Kumar. (2022). Thermoelectric elastic analysis of bi-directional three-layer functionally graded porous piezoelectric (FGPP) plate resting on elastic foundation. *Forces in Mechanics*, 8, 100112. https://doi.org/10.1016/j.finmec.2022.100112

[13] S. Hashemi, A.A. Jafari. (2020). An analytical study for nonlinear vibration analysis of two-directional functionally graded rectangular plate. *Iranian Journal of Mechanical Engineering Transactions of the ISME*, 21(2).

[14] Q.X. Lieu, D. Lee, J. Kang, J. Lee. (2019). NURBS-based modeling and analysis for free vibration and buckling problems of in-plane bi-directional functionally graded plates. *Mechanics of Advanced Materials and Structures*, 26(12), 1064-1080. https://doi.org/10.1080/15376494.2018.1430273

[15] Q.X. Lieu, S. Lee, J. Kang, J. Lee. (2018). Bending and free vibration analyses of in-plane bi-directional functionally graded plates with variable thickness using isogeometric analysis. *Composite Structures*, 192, 434-451. https://doi.org/10.1016/j.compstruct.2018.03.021

[16] S. Li, S. Zheng, D. Chen. (2020). Porosity-dependent isogeometric analysis of bi-directional functionally graded plates. *Thin-Walled Structures*, 156, 106999. https://doi.org/10.1016/j.tws.2020.106999

[17] H.-Q. Tran, V.-T. Vu, M.-T. Tran. (2023). Free vibration analysis of piezoelectric functionally graded porous plates with graphene platelets reinforcement by pb-2 Ritz method. *Composite Structures*, 305, 116535. https://doi.org/10.1016/j.compstruct.2022.116535

[18] K.-S. Na, J.-H. Kim. (2004). Three-dimensional thermal buckling analysis of functionally graded materials. *Composites Part B: Engineering*, 35(5), 429-437. https://doi.org/10.1016/j.compositesb.2003.11.013

[19] B. Uymaz, M. Aydogdu. (2007). Three-dimensional vibration analyses of functionally graded plates under various boundary conditions. *Journal of Reinforced Plastics and Composites*, 26(18), 1847-1863. https://doi.org/10.1177/0731684407081351

[20] B. Uymaz, M. Aydogdu. (2013). Three dimensional mechanical buckling of FG plates

with general boundary conditions. *Composite Structures*, 96, 174-193.https://doi.org/10.1016/j.compstruct.2012.07.033